Understanding part to part variability during directed energy deposition processes using in situ and ex situ process characterization

Niyanth Sridharan

June 5, 2018

CRADA FINAL REPORT
NFE-17-06580

Approved for Public Release.
Distribution is Unlimited.

OAK RIDGE NATIONAL LABORATORY
MANAGED BY UT-BATTELLE FOR THE US DEPARTMENT OF ENERGY

Materials Science and Technology Division
Advanced Manufacturing Office

UNDERSTANDING PART TO PART VARIABILITY DURING DIRECTED ENERGY DEPOSITION PROCESSES USING *IN SITU* AND *EX SITU* PROCESS CHARACTERIZATION

Authors
Niyanth Sridharan
Justin S. Baba
Brian H. Jordan
Ralph B. Dinwiddie
Ryan R. Dehoff

Date Published:
June 5, 2018

Approved For Public Release

CONTENTS

LIST OF FIGURES

ACKNOWLEDGEMENTS

ABSTRACT

The overall goal of this technical collaboration is the use of in situ and ex situ characterization techniques to understand part to part variability in Ti-6Al-4V parts fabricated using directed energy deposition (DED) process, and subsequently qualify parts fabricated using AM. The primary goal of the Phase-1 of this CRADA was to demonstrate the feasibility of capturing the above changes using a combination of high speed stereo imaging and in situ monitoring using two wavelength pyrometers. The in situ monitoring was then correlated using ex situ characterization performed using optical microscopy. The results from phase-1 clearly show that changes to the process and shielding gases have a significant impact on the geometric conformity of the build and the build layer height. The results from phase-1 show that in addition to using IR thermography as a tool to measure the temperature and gradients, we could use it to monitor the build topography and the layer height and use the information to develop closed loop control systems. The phase-1 results show that there is a narrow zone under which the process must operate in order to be "passively stable" or autocorrect for over building. In addition, the results demonstrate that when operated within this range the build autocorrects and there is a drastic reduction in the interlayer lack of fusion defect formation.

1. UNDERSTANDING PART TO PART VARIABILITY DURING DIRECTED ENERGY DEPOSITION PROCESSES USING *IN-SITU* AND *EX-SITU* PROCESS CHARACTERIZATION

This phase 1 technical collaboration project (MDF-TC-17-116) was begun on June 23, 2017 and was completed on June 5, 2018. The collaboration partner Rolls-Royce corporation is a large business. Results show that by utilizing the two wavelength camera in conjunction with a high speed camera it is possible to correlate the effect of changing the shielding gas flow rates on the melt pool temperature. In addition, the transience in the melt pool as an effect of changing the programed movement of the head along the Z axis after the deposition of the laser was also analyzed.

1.1 BACKGROUND

The widespread adoption of the laser directed energy deposition technique is restricted primarily by the lack of certification and standards due to significant part-to-part variability. Rolls-Royce is interested to understand the source of this variability, and potentially develop techniques to control this phenomenon. The directed energy deposition (DED) process has several controllable variables which include, but are not limited to, the laser power, travel speed, scan pattern, powder feed rate, and shielding gas flow rates/velocity. The major source of variability in the deposition process that has not been documented extensively is the one that occurs as a result of the feedstock quality and the influence of process gas flow rates on the powder stream characteristics which is what this partnership aimed to address. Phase-1 focuses on the developing in situ and ex situ techniques to measure and capture the various process dynamics such a powder flow characteristics and the influence of such a change on the melt pool size. Ex situ characterization followed to validate the in situ data. Based on the success of phase 1, phase 2 would evaluate the sources of variability arising from feedstock, the effects of interlayer dwell time on the build quality. In addition the phase 2 would seek to integrate additional sensors and cameras to achieve a spatial and temporal distribution of temperature in 3D space. In addition, imaging techniques will be developed to relate thermal field to

microstructural features.

1.2 TECHNICAL RESULTS

The laser directed energy deposition process utilizes a laser focused on a substrate material creating a melt pool into which powder is "sprayed" co-axially or via an off axis technique to deposit material. The laser head then rasters in the X-Y plane at a programmed velocity and the entire assembly moves up in Z direction once the layer is complete [1], [2]. While the process has the ability to fabricate complex shapes, the parts could have significant defect content and hence exhibit a scatter in the associated mechanical properties [1], [2]. Eliminating defects in components fabricated using additive manufacturing necessitates the optimization of process parameters including, but not limited to, laser power, travel speed, powder feed rate and hatch spacing [1]–[5].

In addition to these parameters, one of the most critical parameters which determines the geometric conformity and propensity to defect formation is the stand off distance [6][7]. The stand off distance also controls the height of the cladding layer. The height of the cladding layer is important from the perspective of geometric conformity. Ideally the height of each cladding layer should be strictly equal to the thickness of the slice sliced from the CAD model (the distance the nozzle moves up in Z) and some difference always exists due to the perturbations in the process [7]. However, if no corrective action was taken, these differences would eventually magnify making the accuracy in the Z direction worse than that in the X and Y direction by almost an order of magnitude. This overbuilding/underbuilding would lead to the formation of lack of fusion defects by altering the focus of the laser leading to improper melting [8]. Controlling the height of the single layer strongly depends on the stand off distance which controls the amount of powder entering the melt pool [9].

The amount of powder entering the melt pool is determined also by the diameter of the powder stream and the melt pool size. In addition, the velocity of the powder particles, which is function of the gas flow rates is also an important contributing factor controlling the deposit quality, surface finish and geometric conformity [9]. Increasing the flow rate of the gases lead to a corresponding increase in the velocity of the powder particles resulting in a low capture efficiency due to the powder rebounding from the surface [9] [10][11]. Therefore, understanding this relationship necessitates a detailed understanding of the influence of shaping and shielding gases on the powder cloud formation and relate this to the changes in the melt pool. This could be achieved by using a combination of in situ and ex situ characterization techniques, which is the focus of the present phase-1 study. To understand this, a detailed in situ characterization and validation needs to be performed using advanced in situ and ex situ tools. Therefore, experiments performed had three components
   1. *Powder stream characterization:* Characterize the effect of process gases on powder stream
   2. *In situ melt pool characterization:* Characterize the effect of the powder stream on melt pool
   3. *Ex situ characterization:* Characterize the influence of process parameters on defect density

1.2.1 Characterization of powder stream characteristics using high speed imaging:

The characteristics of the powder stream was evaluated for multiple combinations of the process gas. The powder flow rate was kept constant at 6 gpm while the cover gases, carrier gas, shaping, and nozzle gases were modified for each condition. The various conditions used are documented in table-1. The effect of the changes to the powder stream was evaluated using a PHANTOM high-speed camera utilizing a 135 mm lens set at f/2.0. The powder stream was captured at a frame rate of 7900 Hz with an exposure time of 120 microseconds.

To capture the entire section of the powder stream in 3 dimensions, stereo imaging was performed where two mirrors mounted at an oblique angle of 110º were used to capture the powder stream. The

2

two images were then super imposed to produce a 3-dimensional stereo image of the captured powder stream. The major parameters measured were the geometry of the powder stream itself, the distribution of the powder in the stream as a function of the vertical distance from the nozzle, the velocity of the powder particles in the powder stream and the included angle of the stream.

Table:1 Process parameters used for powder stream characterization

	Gas flow rates				Powder stream measured results			
	Cover Gas (lpm)	Carrier Gas (lpm)	Shaping Gas (lpm)	Nozzle Gas (lpm)	Focus	Waist	Capture angle	Velocity (mm/s)
1	6	3	18	18	12.82	8.93	32.75	95.24
2	6	3	*12*	18	13.44	8.54	28.36	61.0
3	6	3	12	*14*	*12.87*	*8.37*	*30.54*	*67.32*
4	*12*	3	12	14	13.19	8.16	26.43	45.82
5	6	*6*	12	14	12.90	9.25	25.06	32.87
6	*3*	*3*	12	14	N/A	N/A	N/A	N/A

The background subtracted high speed camera images for all the 6 conditions are presented in figure-1(a)-(f).
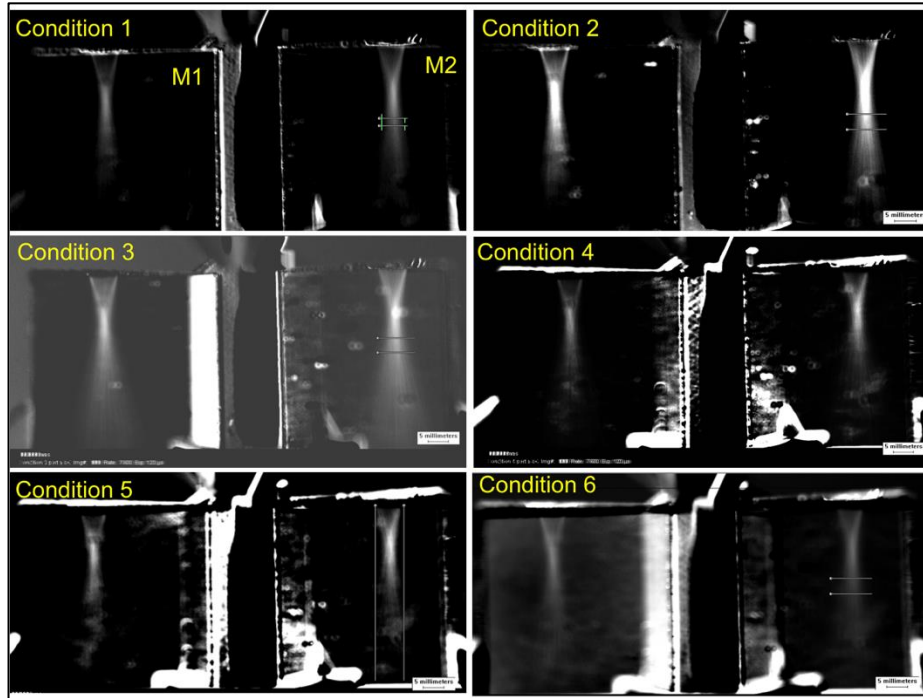
Figure 1: Powder flow distribution (raw unprocessed images from the two mirrors (M1 and M2) used for stereo imaging) for the various conditions shown (a) Condition 1 (b) Condition 2 (c) Condition 3 (d) Condition 4 (e) Condition 5 (f) Condition 6.

The corresponding reconstructions in three dimensions are presented in figure 2. Figure 2 shows the contour of the powder flow. The figure clearly shows that the focus point of the cloud and the waist diameter varies strongly as a function of the process gases. The figure clearly shows that the peak concentration of the powder occurs at a distance close to 12 mm from the nozzle. Therefore,

operating the system at a stand off of 12 mm from the substrate would be ideal to maximize the powder capture efficiency. In addition, controlling the working distance will effect the laser focus, which changes the laser spot size, and thereby modulates mass capture efficiency. The results presented in table-1 show that the maximum particle velocity occurred for condition 1 with an average velocity of 95.24 mm/s and the minimum particle velocity occurred for condition 5 with an average velocity of 32.87 mm/s. While it is clear that condition 1 will have the highest velocity, since the this had the maximum flow rate, the reason as to why condition 5 and not condition 3 has the lowest velocity is surprising. One may expect condition 3 to have the lowest particle velocity since overall condition 3 has the least flow rates of the gases. However, a detailed analysis and more extensive design of experiment study with powders procured from multiple vendors will be performed in the phase 2 of this work.
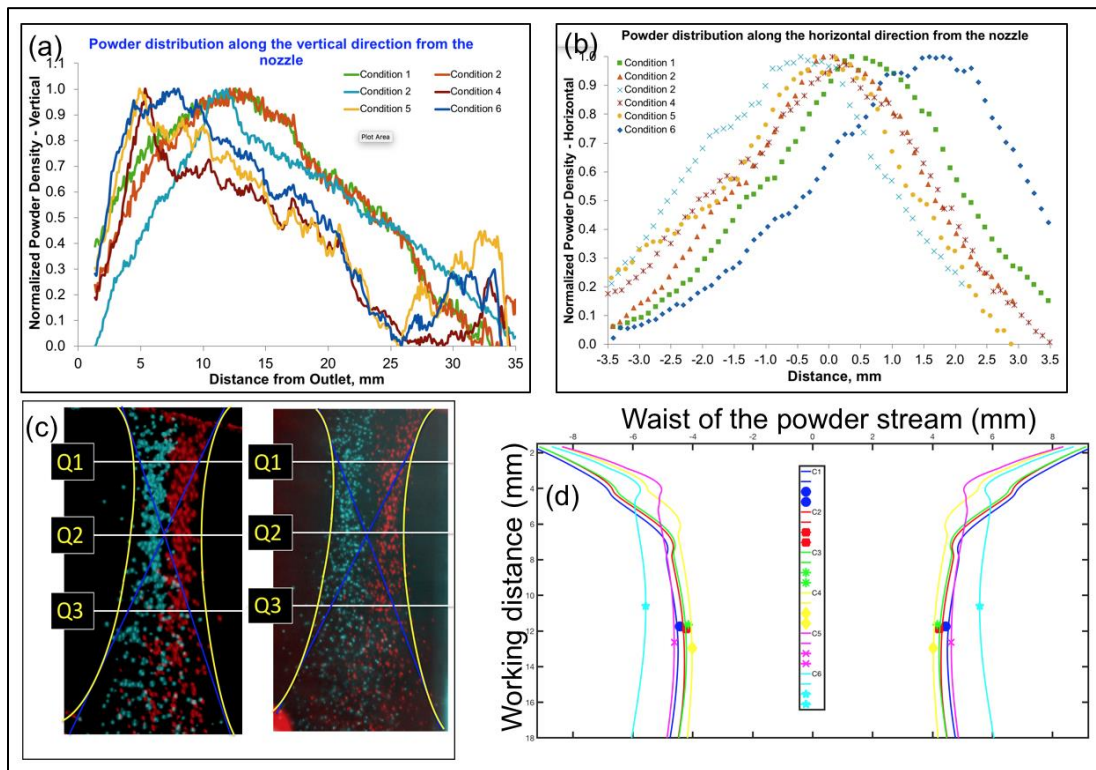
Figure 2: Powder distribution (a) along the vertical direction from the nozzle and (b) Powder distribution along the horizontal direction at 12.5 mm from the nozzle (c) Stereo imaging of the powder flow in condition 1 and condition 6 (d) Contour of the powder cloud distribution.

1.2.2 In situ melt pool characterization:

In order to fabricate defect free parts in an industrial set up using Laser DED, the process dynamics need to be mapped and understood. One method to ensure a robust control is to implement a "passive control" by maintaining a constant working distance. However, the challenge is that there is no explicit method to maintain the same working distance throughout the course of fabrication of the build, which then leads to changing capture efficiency during the fabrication of the build. To study the influence of the processing conditions on the melt pool, builds were fabricated using a constant laser power of 600W and 600 mm/min and a powder feed rate of 6 grams per minute with a hatch spacing of 0.6 mm. The other parameters were systematically varied by changing process parameters in accordance to table-1. In addition, the programed layer height (the preset distance the nozzle moves

4

in the Z direction after deposition of a layer) was also altered just for one case from 1.5 mm to 1 mm. The layer height was selected based on the observed bead height which was slightly higher than 1.5 mm. By having the layer height at 1mm the effective working distance of the build moves into the regime which is passively stable. The parameters used to fabricate the builds are summarized in table-2.

Table 2: Summarizing the process parameters used to fabricate builds

Trial	Cover Gas (lpm)	Carrier Gas (lpm)	Shaping Gas (lpm)	Nozzle Gas (lpm)	Laser power (W)	Travel speed (mm/ min)	Hatch spacing (mm)	Powder feed rate	Layer height (mm)
1	6	3	18	18	600	600	0.6	6	1.0
2	6	3	18	18	600	600	0.6	6	1.5
3	6	3	*12*	18	600	600	0.6	6	*1.5*
4	6	3	12	*14*	600	600	0.6	6	1.5
5	*12*	3	12	14	600	600	0.6	6	1.5
6	6	*6*	12	14	600	600	0.6	6	1.5
7	*3*	*3*	12	14	600	600	0.6	6	1.5

In order to characterize the changes to the melt pool as a function of the shaping gases, a Stratonics THERMAVIZ camera was used. The frame rate used was 5Hz. The camera was mounted at an angle of 30° from the vertical as shown in the schematic. The raw images from the camera were then post processed to extract the melt pool size in pixels, and also to calculate the melt pool centroid location. As depicted in Fig. 3, beginning from left to right, first the full field images for the two imaging wavelengths are separated. Next, a region-of-interest (ROI) that encompasses the full melt pool is automatically detected and then the raw images are cropped. Finally, a binary conversion is performed to identify and extract the boundaries of the melt-pool for quantitative analysis that provides output parameters of melt-pool area and center-of-gravity (COG) coordinates. A screen shot of the analysis is shown in figure 3.
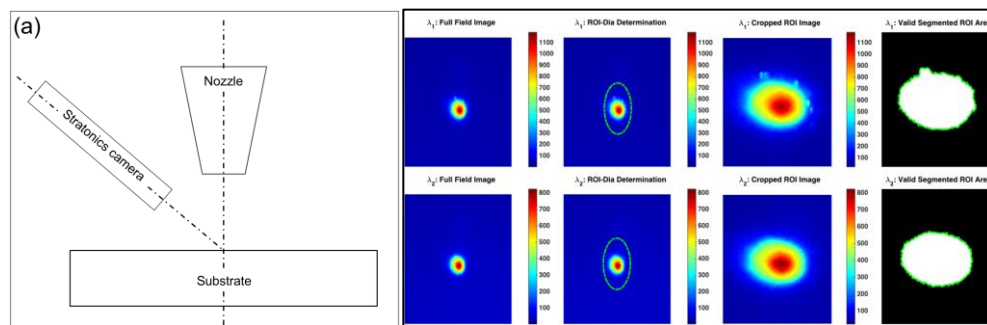
Figure 3: (a) Schematic illustration of the location of the camera with reference to the vertical axis (b) Segmentation and analysis performed on the melt pool to extract the melt pool area and the centroid location.

The melt pool area was expected to change as a function of the process gas flow rates since alterations to the process gas flow rates changes the velocity of the powder particle, which could stochastically disrupt the surface tension of the molten material leading to changes in the melt pool sizes. In particular, the velocity of the carrier gas flow rate was found to have a profound influence on the melt pool in a previous study. The melt pool area was extracted using the procedure described above, and the results are plotted in figure 4. While the prima facie evidence clearly shows significant differences in the melt

pool size and geometry a detailed explanation for these phenomena is currently beyond the scope of the Phase-1 and would be conducted in the Phase-2 of this work.

Figure 4: Melt pool areas for builds fabricated for conditions 2 thru' 6 clearly showing the minor differences.

In addition, the difference in the melt pool area for the sample fabricated with a layer height of 1 mm and 1.5 mm are sho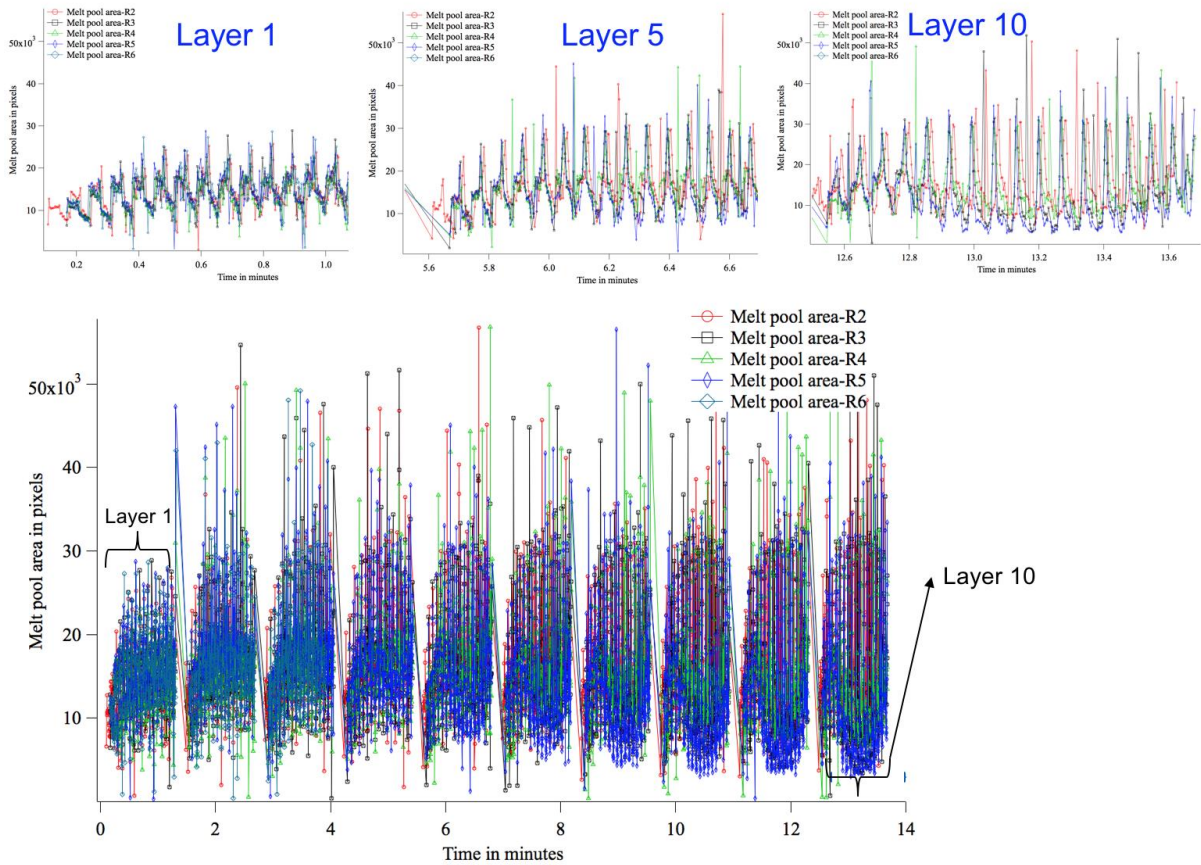wn in figure 5. Note that the initially the melt pool sizes are approximately the same. However, as the build height increases the melt pool size for the builds fabricated with a layer height of 1 mm starts to decrease. This could be related to the fact that the build increases in height faster than the head movement along the Z. This consequently results in laser getting defocused thereby decreasing the build height. This shows that for the present set of operating conditions by maintaining the layer height of 1mm the build enters a zone of "passive stability" thereby autocorrecting for the build height. In addition, the powder capture efficiency also reduces significantly as the stand off distance changes. This is clearly illustrated by the plot shown in figure 6. Figure 6 clearly shows the plot between the time and the centroid of the melt pool. The 30° angle with which the camera is mounted allows a field of view to track the height of the melt pool as well. The centroid corresponds to the location of the melt pool in the X, Y space. The centroid varies directly with the height of the layer. The higher the layer, the lower the centroid value (this is due to the way the system is setup). The difference in the centroid locations between the builds fabricated with a 1 mm and 1.5 mm layer height is shown. The plot clearly shows that the builds fabricated with 1 mm layer height and 1.5 mm show the same layer height for the first few layers. While the layer height of the builds fabricated with a 1 mm layer height then reaches a maximum and then stabilizes the layer height of the samples fabricated using a 1.5 mm layer height starts to increase continuously and

finally moves out of the frame. This is because the laser head and camera are moving away quicker from the top of the build for the sample fabricated with a layer height of 1.5 mm.
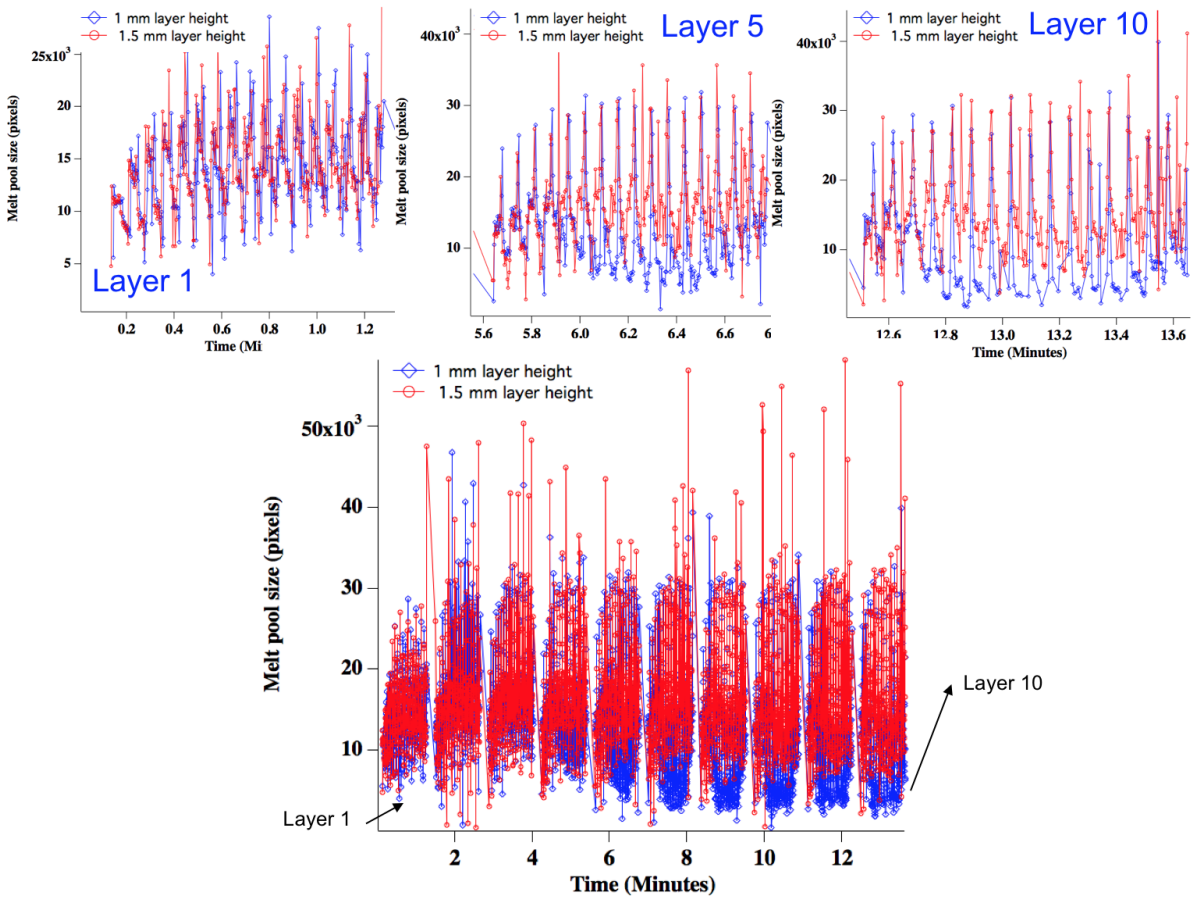

Figure 5: Changes in melt pool dimensions as a function of the layer height.
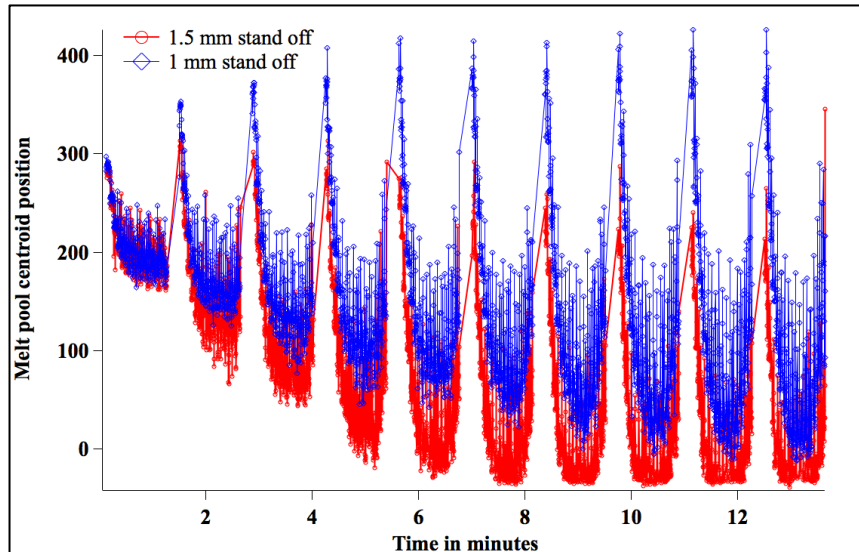

Figure 6: Changes in layer height as a function of the programmed pre set height. The blue corresponds to samples fabricated with a 1mm layer height and the red corresponds to the samples fabricated with a

1.5 mm layer height.

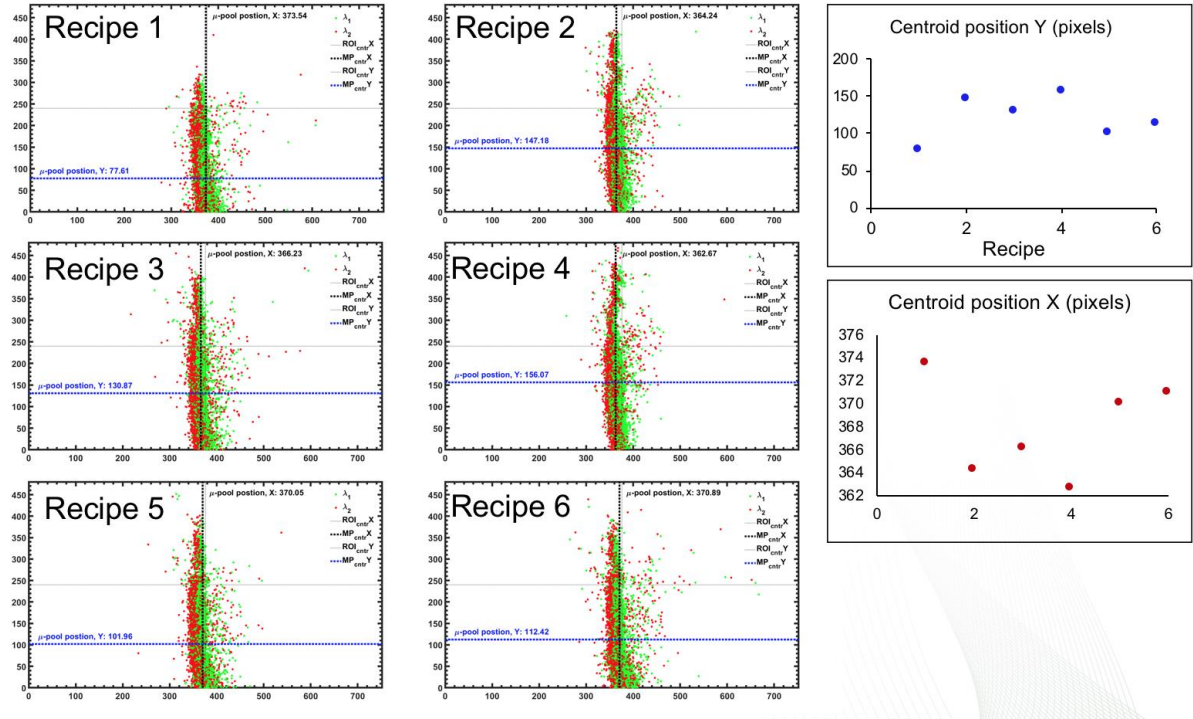The average centroid location of all the builds are summarized in figure 7.

Figure 7: Shows the location of the average centroid representing the build height as a function of the processing conditions.

Figure 7 clearly shows that the average height of all the samples fabricated with different gas flow conditions also have different layer heights implying that this has a strong effect on the powder capture efficiency. However, a more in depth characterization and study is required to exactly study this aspect.

1.2.3 Ex situ characterization:

Following fabrication the parts were then sectioned to examine the defects in the part using optical microscopy. The results are summarized in figure 8 and the build heights are presented in table 3. Note the curvature on the top of the builds. This curvature is a result of the excessive powder capture in the middle of the build and lower capture at the edges. In addition, the layers have severe lack of fusion defects between the layers. The side marked S corresponds to the start of the raster direction of the laser and the side marked F is the end of the raster. Note that the lack of fusion is due to the excessive powder capture leading to insufficient melting. However, the start of the builds where the layer thickness is lower do not have significant lack of fusion. Figure 9 shows the difference between the samples fabricated with a layer height of 1 mm and 1.5 mm. The data clearly validates the previous results that operating the laser with a layer height of 1mm auto corrects for overbuilding. In addition, since the capture efficiency is decreased the layer thickness decreases leading to a reduction in the lack of fusion defects. On comparing the observed optical micrograph of the 1 mm layer height sample to the in situ data it is clear that the layer height increases for the first three layers which is where the bulk of the lack of fusion defects occur. As the process moves towards "passive stability" the amount of the lack of fusion defects decrease.
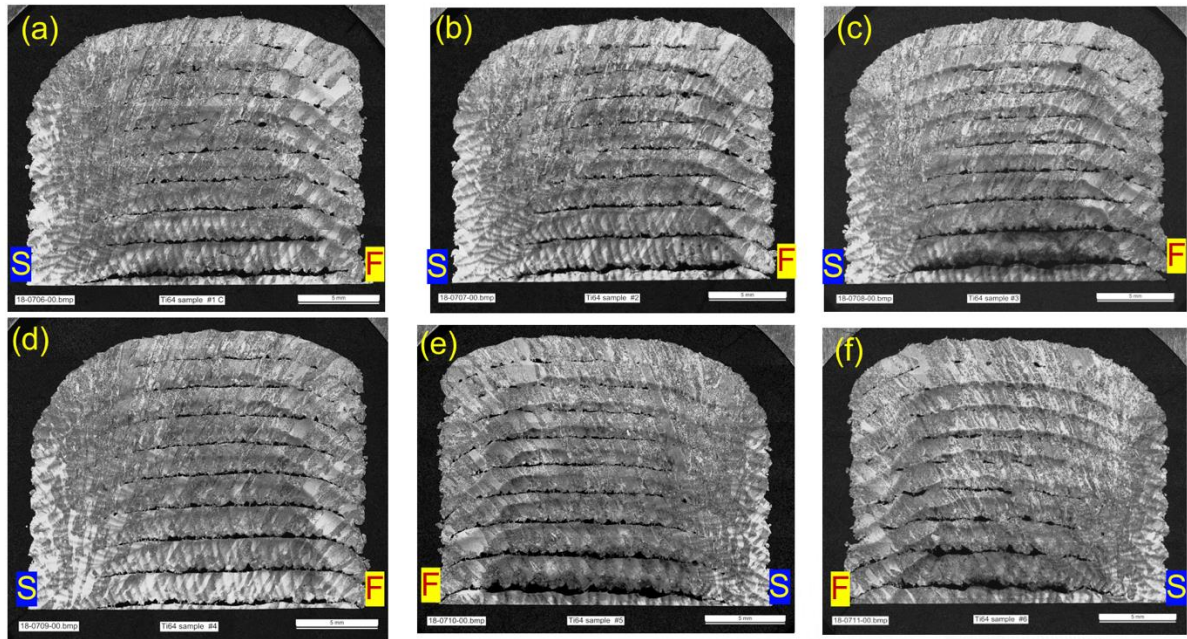
Figure 8: Shows the cross section images of the samples fabricated using (a) recipe 1 (b) recipe 2 (c) recipe 3 (d) recipe 4 (e) recipe 5 (f) recipe6.

Table 3: The measured build height for all the conditions

| Cover Gas (lpm)	Carrier Gas (lpm)	Shaping Gas (lpm)	Nozzle Gas (lpm)	Laser power (W)	Travel speed (mm/min)	Hatch spacing (mm)	Powder feed rate	Layer height (mm)	Build height (mm)
6	3	18	18	600	600	0.6	6	1.0	12.778±0.03
6	3	18	18	600	600	0.6	6	1.5	16.72±0.056
6	3	*12*	18	600	600	0.6	6	*1.5*	16.82±0.22
6	3	12	*14*	600	600	0.6	6	1.5	17.62±0.09
12	3	12	14	600	600	0.6	6	1.5	16.32±0.26
6	*6*	12	14	600	600	0.6	6	1.5	17.13±0.1
3	*3*	12	14	600	600	0.6	6	1.5	17.771±0.45

9
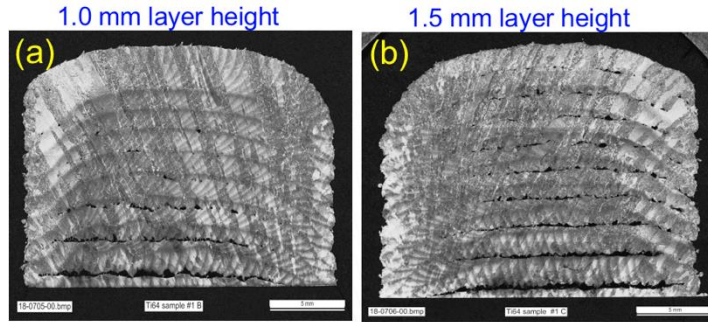
Figure 9: Shows the cross section images of the samples fabricated using (a) recipe 1 with a 1.0 mm layer height (b) recipe 1 with a 1.5 mm layer height.

1.3 IMPACTS

This work has demonstrated the potential of in situ process monitoring to investigate the build to build variability in Ti-6Al-4V parts fabricated using directed energy deposition (DED) process. The phase-1 focused on demonstrating the feasibility of setting up monitoring systems that can effectively capture the changes in the powder cloud formation and link it to the melt pool dynamics and relate it to the propensity to defect formation. However, the study has not developed any techniques to accurately detect porosity or lack of fusion or investigated the differences between feedstock suppliers. These aspects will be the focus of the phase 2 of this program.

1.3.1 Subject Inventions

There are no subject inventions associated with this CRADA.

1.4 CONCLUSIONS

As stated in the previous sections, the goal of the phase 1 of this technical collaboration program was to understand the feasibility of utilizing in situ and ex situ process characterization techniques to identify the sources of build variability. The results clearly show that minor changes to the process gas flow rates affect the powder particle velocity and powder cloud distribution. The spatial and temporal variations were captures using a two wavelength pyrometer which clearly showed the influence of the gas flow rates on the melt pool shape/size and geometry. However, the most important effect was the influence of the changing the programmed layer height (the distance that the head moves up in Z after the deposition of a layer). A change in the layer height from 1.5 mm to 1.0 mm resulted in a dramatic decrease in lack of fusion defects due to the open loop control system inherent to the process. While this study has shown the feasibility of performing such a study the design of experiment matrix is not exhaustive and a more exhaustive study of the parameters need to be performed. In addition, the influence of the powder feed stock on the formation of defects in the builds needs to be evaluated.

2. ROLLS-ROYCE CORPORATION. BACKGROUND

Rolls-Royce is a global company providing highly efficient integrated power and propulsion solutions. Our power systems are predominantly used in aerospace, marine, energy and off-highway

applications. We are one of the world's leading producers of aero engines for large civil aircraft and corporate jets. Rolls-Royce is well established in the marine sector where we design vessels and integrate power systems. We have a growing presence in civil nuclear power as well. Our MTU brand is world-renowned in high-speed diesel engines powering applications as diverse as rail locomotives and luxury yachts. We support our customers through a worldwide network of offices, manufacturing and service facilities.

REFERENCES

[1]   S. M. Thompson, L. Bian, N. Shamsaei, and A. Yadollahi, "An overview of Direct Laser Deposition for additive manufacturing; Part I: Transport phenomena, modeling and diagnostics," *Addit. Manuf.*, vol. 8, pp. 36–62, 2015.

[2]   N. Shamsaei, A. Yadollahi, L. Bian, and S. M. Thompson, "An overview of Direct Laser Deposition for additive manufacturing; Part II: Mechanical behavior, process parameter optimization and control," *Addit. Manuf.*, vol. 8, pp. 12–35, 2015.

[3]   K. Shah, A. J. Pinkerton, A. Salman, and L. Li, "Effects of melt pool variables and process parameters in laser direct metal deposition of aerospace alloys," *Mater. Manuf. Process.*, 2010.

[4]   Y. Li, H. Yang, X. Lin, W. Huang, J. Li, and Y. Zhou, "The influences of processing parameters on forming characterizations during laser rapid forming," *Mater. Sci. Eng. A*, 2003.

[5]   G. Zhu, D. Li, A. Zhang, G. Pi, and Y. Tang, "The influence of laser and powder defocusing characteristics on the surface quality in laser direct metal deposition," *Opt. Laser Technol.*, 2012.

[6]   H. Tan *et al.*, "Process mechanisms based on powder flow spatial distribution in direct metal deposition," *J. Mater. Process. Technol.*, 2018.

[7]   L. Peng, J. Shengqin, Z. Xiaoyan, H. Qianwu, and X. Weihao, "Direct laser fabrication of thin-walled metal parts under open-loop control," *Int. J. Mach. Tools Manuf.*, 2007.

[8]   G. Zhu, D. Li, A. Zhang, G. Pi, and Y. Tang, "The influence of laser and powder defocusing characteristics on the surface quality in laser direct metal deposition," *Opt. Laser Technol.*, vol. 44, no. 2, pp. 349–356, Mar. 2012.

[9]   R. R. Dehoff *et al.*, "Demonstration of thermal control, microstructure control, defect mitigation and process parameter database generation for Ti-6Al-4V Direct Digital Manufacturing-Understanding defect mitigation and process parameter database generation for direct digital m," 2015.

[10]   J. Lin and W. M. Steen, "Design characteristics and development of a nozzle for coaxial laser cladding," *J. Laser Appl.*, 1998.

[11]   J. Lin, "Simple model of powder catchment in coaxial laser cladding," *Opt. Laser Technol.*, 1999.